

Peptide-drug conjugate GnRH-sunitinib targets angiogenesis selectively at the site of action to inhibit tumor growth

Orestis Argyros¹, Theodoros Karampelas¹, Xenophon Asvos², Aimilia Varela³, Nisar Sayyad², Athanasios Papakyriakou⁴, Constantinos H. Davos³, Andreas G Tzakos², Demosthenes Fokas⁵, Constantin Tamvakopoulos¹

¹Division of Pharmacology-Pharmacotechnology, Clinical, Experimental Surgery & Translational Research Center, Biomedical Research Foundation Academy of Athens (BRFAA), Athens, 11527, Greece

²Department of Chemistry, Organic Chemistry and Biochemistry, University of Ioannina, Ioannina, 45110, Greece

³Cardiovascular Research Laboratory, BRFAA, Athens, 11527, Greece

⁴Laboratory of Chemical Biology of Natural Products and Designed Molecules, Institute of Physical Chemistry, N.C.S.R “Demokritos”, Athens, 15310, Greece

⁵Laboratory of Medicinal Chemistry, Department of Materials Science and Engineering, University of Ioannina, Ioannina, 45110, Greece

Running Title: A potent Sunitinib-GnRH conjugate for tumor targeting

Keywords: Angiogenesis, gonadotropin releasing hormone receptor, sunitinib analogs, tumor targeting

Financial Support

This work was co-funded by the Greek Ministry of Education, National Strategic Reference Framework (NSRF) 2007-2013 under grant "PostDoc - DENTAD-PROCAT" (LS7-1682/17156/6.12.10).

***Address correspondence to:**

Dr. Constantin Tamvakopoulos,
Clinical, Experimental Surgery, & Translational Research Center
Division of Pharmacology-Pharmacotechnology
Biomedical Research Foundation, Academy of Athens, Athens, 11527, Greece.
E-mail: ctamvakop@bioacademy.gr, Phone: +30-210-6597475

Disclosure of Potential Conflicts of Interest

The authors declare that they have no conflict of interest to disclose

Abstract

The potential to heighten the efficacy of antiangiogenic agents was explored in this study based on active targeting of tumor cells overexpressing the gonadotropin-releasing hormone receptor (GnRH-R). The rational design pursued focused on five analogs of a clinically established antiangiogenic compound (sunitinib) from which a lead candidate (SAN1) was conjugated to the targeting peptide [D-Lys⁶]-GnRH, generating SAN1GSC.

Conjugation of SAN1 did not disrupt any of its antiangiogenic or cytotoxic properties in GnRH-R expressing prostate and breast tumor cells. Daily SAN1GSC treatments in mouse xenograft models of castration-resistant prostate cancer resulted in significant tumor growth delay compared to equimolar SAN1 or sunitinib alone. This efficacy correlated with inhibited phosphorylation of AKT and S6, together with reduced Ki-67 and CD31 expression. The superior efficacy of the peptide-drug conjugate was also attributed to the finding that higher amounts of SAN1 were delivered to the tumor site (~4-fold) following dosing of SAN1GSC compared to equimolar amounts of non-conjugated SAN1.

Importantly, treatment with SAN1GSC was associated with minimal hematotoxicity and cardiotoxicity based on measurements of the left ventricular systolic function in treated mice.

Our results offer preclinical proof of concept for SAN1GSC as a novel molecule that selectively reaches the tumor site and downregulates angiogenesis with negligible cardiotoxicity, thus encouraging its further clinical development and evaluation.

Introduction

The concept of generating novel cancer therapeutics that target specific cell-surface receptors has been a driving force of drug development over the past few years (1-3). This idea is based on evidence that certain cell-surface receptors in malignant cells are either mutated or overexpressed (*e.g.*, EGFR, HER2/neu, GnRH-R), compared to normal cells (4-6) and that these alterations provide “druggable” opportunities. We recently demonstrated the successful targeting of gonadotropin releasing hormone receptor (GnRH-R) in GnRH-R positive prostate cancer (CaP) using a conjugate of a GnRH peptide linked to the cytotoxic drug gemcitabine (7). These studies were inspired by evidence of a doxorubicin based conjugate (AN152) that has now advanced to phase III clinical trials for various solid malignancies (8,9).

The GnRH-R is primarily located in the pituitary gland (10,11) but upregulation of its expression has been reported in prostate, breast and other cancers (10,12) which persists despite prolonged exposure to GnRH agonists (6). Interestingly an antiproliferative role has also been reported for GnRH, providing additional opportunities for the treatment of tumors by directly affecting cancer cells apart from the pituitary (13,14).

Tumor growth depends on the ability of new vessels to sprout in a process called angiogenesis. Numerous antiangiogenic agents have been developed which inhibit the phosphorylation of certain receptors like the vascular endothelial growth factor receptors (VEGFRs) types 1/2 and platelet-derived growth factor receptors (PDGFR- α/β) (15). A typical example of a clinically successful antiangiogenic agent is sunitinib, an orally available small molecule that inhibits phosphorylation of several receptor tyrosine kinases (RTKs) including VEGFRs-1/2, PDGFR- α/β , KIT and FLT3, with an average IC₅₀ below 100 nM (16,17). Clinical trials of sunitinib in

tumors, such as prostate (18) and breast cancer (19) were initiated based on successful preclinical evidence (16,20) but were halted in phase III, despite prolongation of progression free survival, due to the lack of statistically significant overall survival in patients. Experience with sunitinib in the clinic demonstrated that a considerable subset of sunitinib treated patients develop left ventricular (LV) dysfunction and overt heart failure (21,22).

Based on the findings of the above studies, we surmised that increased specificity of sunitinib delivery at the site of action through conjugation to a targeting agent may lead to improved efficacy while minimizing peripheral toxicities. We decided to pursue this concept by generating novel GnRH-based molecules conjugated to sunitinib, with the prospect of exploiting the additional antiproliferative effects of the GnRH peptide itself.

Conjugation of sunitinib to a targeting group is challenging due to the possibility of altering the potency and pharmacokinetics of the pharmacophore. Few groups have experimented with the generation of sunitinib analogs (23-29), based on cocrystallization studies (30) that revealed indolin-2-one core as the moiety of the drug involved in kinase inhibition. Substitutions at the C4 position might serve as a handle for improving pharmaceutical properties as shown by toceranib (26). Based on the above structure activity relationship studies, some sunitinib analog conjugates have been synthesized and evaluated either as imaging tools (27) or as lysozyme based targeting agents (25), but to our knowledge no conjugation to a peptide moiety has been reported.

Herein, we present the results of preclinical studies for a GnRH-sunitinib based conjugate (called SANIGSC), generated after the evaluation of various novel sunitinib analogs (designated as SANs 1-5). The analogs were designed to be linkable

to a variety of peptides while maintaining their antiangiogenic properties, a desired feature that expands their translational applications. Enhanced efficacy, minimal toxicity and improved biodistribution properties of SAN1GSC were shown, in comparison to its unconjugated derivative (SAN1) or sunitinib.

Materials and Methods

Chemicals, synthesis and Characterization of compounds

Sunitinib was purchased from Selleckchem (Selleckchem, USA) and [D-Lys⁶]-GnRH from Proteogenix (Schiltigheim, France). All other chemicals and biologicals, unless stated otherwise were purchased from Sigma-Aldrich (Sigma-Aldrich, Munich, Germany). The synthesis of SAN1-SAN5 (Figure 1A) and of SAN1GSC (Figure 4A) is presented in the supplementary information section (S.I.1 and S.I.3). All molecules were analyzed by Mass Spectrometry (MS) in order to obtain the key spectral features necessary for their quantification in blood and tissue as described previously (7,31). Total polar surface area and clogP values, were predicted by Chemdraw Ultra (v10, PerkinElmer Informatics, USA).

Computational methods

Detailed docking and molecular dynamic analysis for all the compounds was performed as described in the S.I.2.

In vitro evaluation of compounds

The trans-phosphorylation activity of VEGFR-2, PDGFR- β , KIT, FLT3, ribosomal protein S6 kinase (RPS6KB1) and EGFR was evaluated as described before (17). Detailed methods and a list of the kinases used are available in the S.I.4. Cellular inhibition of autophosphorylation of VEGFR-2 and PDGFR- β was performed as described previously (32). Detailed methods are available in the S.I.5. For cellular

studies, cells were used within six months of purchase or authentication and were cultured as instructed by the American Type Culture Collection (LGC Standards, Germany). The HCC1954 cell line was obtained from ATCC and HUVEC from Life Technologies, UK. The DU145, PC3 and NIH/3T3 cells were authenticated by short tandem repeat profiling (Microsynth, Switzerland). WPE1-NB26-3 cells were a kind gift from Professor Robert Millar (University of Pretoria, SA)

Pharmacokinetic analysis

All animal procedures were approved by the Bioethical Committee of BRFAA based on the European Directive 86/609. Equimolar (17 $\mu\text{mol/Kg}$) dosing solutions for each compound were prepared in 20% 2-hydroxypropyl β -Cyclodextrin in water (HP-b-CD), except for SANIGSC that was solubilized in saline. All compounds were administered intraperitoneally (IP) in male NOD/SCID mice (8-10 weeks, n=4, from Charles River, Italy) and blood samples were collected and prepared as described previously (7).

In vivo efficacy of sunitinib, SAN1 and SANIGSC

NOD/SCID mice were injected in each flank with 3×10^6 DU145 cells, a castration-resistant CaP (CRPC) cell line. Treatment was initiated when tumors reached 200 mm^3 by daily IP administrations of sunitinib or equimolar doses of SAN1 (100 $\mu\text{mol/Kg}$). Control mice received saline or HP-b-CD. In separate experiments, mice were treated with equimolar amounts (9.17 $\mu\text{mol/Kg}$) of SANIGSC, SAN1 and [D-Lys⁶]-GnRH. Mice were weighed regularly and phenotypic signs of discomfort were monitored as described in the S.I.6. Experiments were terminated after approximately 20 days, at 1h or 2h after the last administered dose by euthanizing the animals under isoflurane anesthesia. Tumors were excised, weighed and prepared for histopathology, immunohistochemistry (IHC), kinase activity and quantification of compounds by

LC-MS/MS.

Immunohistochemistry

Excised tumors were fixed in neutral buffered formalin, paraffin embedded, sectioned and stained against CD31, Ki-67, pS6 and pRPS6KB1. Microvessel density was assessed by counting the number of CD31 positive vessels in a 40x microscope field in a blinded fashion and presented as the amount of blood vessels/mm². Cell proliferation was measured by counting Ki-67 positive cells in a 40x microscope field. Images were acquired by a Leica DFC350-FX camera mounted on a Leica DMLS2 microscope.

In vivo kinase activity

The PathScan RTK signaling array kit (Cell Signaling, UK) was used per manufacturer's direction to detect the phosphorylation status in supernatants from tumor extracts (n=10 for each treatment). Images were analyzed with ImageJ software (v1.28) by loading the image as a gray scale picture. Each kinase array dot was manually selected, normalized and an average intensity for each kinase was calculated as described previously (33).

Toxicity Evaluation

Cardiotoxicity was evaluated through echocardiography as described previously (34) and in S.I.7. Hematotoxicity was assessed as described in the S.I.8.

Statistical analyses

Statistical analyses and calculation of all IC₅₀s were performed by SigmaPlot 12 software. Statistical significance was determined using the Student's two-tailed, two-sample unequal variance distribution *t* test.

Results

Synthesis of SANs

The synthetic route for SANs 1-5 is shown in Figure 1A. These modified versions of sunitinib maintain the RTK inhibition indolin-2-one core while in addition they provide a handle for conjugation to a targeting peptide. Figure 1B depicts the MS features as well as some key properties for all SANs. Although the lipophilicity of sunitinib variants (SANs 1-5) was decreased compared to sunitinib, the polar surface area remained unaffected ($<100 \text{ \AA}^2$) for all SANs, a parameter known to influence cell membrane permeability (35). A representative mass spectrum and LC-MS/MS chromatogram for a chosen analog (SAN1) can be found in S.I.2.

Molecular docking calculations

Molecular docking calculations were performed for the synthesized SANs based on the catalytic domain of three key kinase receptors: VEGFR-2, PDGFR- β and KIT. Estimated inhibition constants K_i (Figure 2A) were in the low nM range, similar to the estimated values of sunitinib. A representative molecular model of SAN1 complexed with VEGFR-2 is shown in Figure 2A and S.I.3.

Biochemical kinase assays

The potency of all SANs was experimentally evaluated in biochemical assays against purified VEGFR-2, PDGFR- β , KIT, FLT3 and presented in Figure 2B. All SANs inhibited the specific RTK targets with IC_{50} values ranging from 20 to 150 nM comparable to sunitinib. The EGFR served as a negative control (concentrations up to 10 μ M did not inhibit EGFR phosphorylation).

Cellular ligand-dependent phosphorylation assay

The inhibition of phosphorylation of VEGFR-2 and PDGFR- β , was further confirmed in HUVEC and NIH/3T3 cells, using a Western blot based cellular ligand-dependent

phosphorylation assay. The calculated cellular IC₅₀ value for sunitinib was 24±12 nM (for VEGFR-2) and 72±19 nM for PDGFR-β respectively. Similar potencies were observed for all SANs with cellular IC₅₀ values ranging from 52-180 nM (Figure 2C).

Cytotoxicity studies

The antiproliferative effect of the five SANs was assessed in three GnRH-R positive CaP cell lines (DU145, PC3, WPE1-NB26-3) one GnRH-R positive breast cancer cell line (HCC1954), in HUVEC and NIH/3T3 cells. Results and comparative IC₅₀ values are presented in Figure 2D. SAN1 proved highly potent in HUVEC and DU145 cell lines (IC₅₀s: 8±4 μM and 11±2 μM respectively), SANs 2-4 showed intermediate efficacies while SAN5 appeared inactive (IC₅₀>100 μM) and was discarded from further evaluation.

Pharmacokinetic evaluation

The most promising molecules (SANs 1-4) were evaluated for their pharmacokinetic parameters in mice. Sunitinib maximum blood concentrations were achieved at 0.25 h (1.5 μM) with an AUC_{0-8h} of 2.51 h x μM. Similarly, SANs 1-4 were rapidly absorbed reaching highest blood concentrations averaging in the range of 0.5 to 2.1 μM at 0.25 to 1 h after dosing (Figure 2E). Following dosing, concentrations of SAN1 peaked at 0.25 h with an AUC_{0-8h}: 1.11 h x μM. Signs of discomfort were observed in mice that received SAN2, discouraging further evaluation. According to the biochemical assays, compound concentrations of approximately 100 nM were needed for the inhibition of the target kinases (Figure 2A-C). Following IP dosing, such levels could be sustained for 4 h post-dose for all the molecules tested. A single IP administration of an efficacious dose of sunitinib (100 μmol/Kg) was the point of reference for subsequent efficacy studies in mice (Figure 2E). Based on the described pharmacokinetic and biological readouts combined with its facile synthetic route,

SAN1 was selected as the lead candidate compound for follow-up efficacy studies in mice.

In vivo antitumor efficacy of SAN1

Mice bearing established DU145 tumors were treated with each molecule at 100 $\mu\text{mol/Kg/day}$ (equivalent to 40 mg/Kg). A significant tumor growth delay was observed in all mice treated with sunitinib (Figure 3A), with the average tumor size at d19 at $312 \pm 123 \text{ mm}^3$ and an average tumor weight of $0.20 \pm 0.08 \text{ g}$ compared to $1181 \pm 105 \text{ mm}^3$ ($p < 0.0001$) and $0.87 \pm 0.51 \text{ g}$ ($p = 0.005$) for vehicle treated mice (Figure 3B). Tumor growth delay was also observed in DU145 xenografted mice treated with equimolar SAN1 (figure 3A), with an average tumor size at d19 of $455 \pm 137 \text{ mm}^3$ ($p < 0.001$ compared to vehicle treated mice). The corresponding average tumor weight at sacrifice was $0.37 \pm 0.19 \text{ g}$ for SAN1 (Figure 3B, $p = 0.005$ compared to vehicle treated mice). Concentrations of sunitinib and SAN1 in blood and tumor tissue were measured at 2 h after the final dose. Sunitinib's blood concentrations were $4.7 \pm 0.1 \mu\text{M}$, whereas levels at tumor tissue were $11.0 \pm 5.0 \mu\text{M}$ (Figure 3C). The values for SAN1 in the tumor tissue were significantly lower at $0.4 \pm 0.2 \mu\text{M}$, but exceeded the IC_{50} level threshold (100 nM) determined for inhibition of phosphorylation of the target kinases. It should be noted that sunitinib is more lipophilic compared to SAN1 (as evident in their clogP values), a property that explains the higher drug accumulation in the tumor tissue over the treatment period.

In vivo target modulation studies

Insights into the molecular mechanism responsible for the observed *in vivo* efficacy of SAN1 were obtained by histological, immunohistochemical and target modulation analysis of tumors harvested from treated and untreated animals. Hematoxylin and eosin stained tissue sections were evaluated by an independent histopathologist who

confirmed that the features of the tumors were consistent with a Gleason score 10, prostatic acinar adenocarcinoma (Figure 3D). Tumors were composed of malignant epithelial cells distributed in solid sheets without glandular formations. The nuclei were pleomorphic, vesicular and contained a prominent nucleolus. Isolated mitotic figures were noted. IHC analysis using antibodies against Ki-67 and CD31 showed a marked reduction in cell proliferation and reduced angiogenesis in sunitinib treated mice and SAN1 treated mice (Figure 3D). The Ki-67 assessed proliferation indices (PI) of mice treated with the compounds of interest were as follows: for sunitinib (100 $\mu\text{mol/Kg}$): $9.1\pm 3.3\%$ ($P<0.001$, treated/untreated PI ratio = 0.176), for SAN1 (100 $\mu\text{mol/Kg}$): $16.8\pm 3.1\%$ ($P<0.001$, treated/untreated PI ratio = 0.325), and for vehicle treated animals $51.7\pm 6.5\%$. Additionally for CD31 the average number of CD31+ cells of mice treated with sunitinib at 100 $\mu\text{mol/Kg}$ and mice treated with SAN1 at 100 $\mu\text{mol/Kg}$ versus vehicle treated mice were 5.3 ± 2.2 , 6.8 ± 1.6 and 34.5 ± 8.9 respectively.

A marked downregulation of pAKT (Ser473), pS6 and pSTAT1 was noted when the phosphorylation status of 39 kinases was investigated in extracts of tumor tissue in drug treated versus vehicle treated mice, consistent with the multikinase phosphorylation inhibition ability of sunitinib and the designed SAN1 analog (Figure 3E).

Generation of SANIGSC

Based on the *in vivo* efficacy profile, SAN1 was selected for conjugation to the [D-Lys⁶]-GnRH targeting peptide by utilizing the free hydroxyl group of SAN1. Prior experience (7) allowed us to implement a succinate linker strategy for SAN1 to [D-Lys⁶]-GnRH, resulting in the SANIGSC molecule as shown in Figures 4A and S.I.3). Molecular docking calculations indicated that SANIGSC could bind to the target

receptors with a predicted $K_i=28$ nM for VEGFR-2, $K_i=65$ nM for PDGFR- β and $K_i=51$ nM for KIT (Figure 4B).

In vitro evaluation of SAN1GSC

Incubation of SAN1GSC with VEGFR-2, PDGFR- β , KIT and FLT3 resulted in the inhibition of phosphorylation of each of the above kinases with respective IC_{50} values of 97 ± 41 , 91 ± 36 , 74 ± 36 and 37 ± 6 nM (Figure 4C). Western blot analysis indicated that SAN1GSC inhibited the phosphorylation of VEGFR-2 and PDGFR- β , with nM potency (38 ± 12 nM for VEGFR-2 and 76 ± 17 nM for PDGFR- β , Figure 4D). Finally, SAN1GSC was equipotent to SAN1 in terms of cellular toxicity in various cell lines with the calculated IC_{50} ranging from 9 to 18 μ M (Figure 4E).

The SAN1GSC mediated GnRH-R activation of the pERK1/2 signaling pathway was investigated by setting-up an indirect method based on the WPE1-NB26-3 cell line. Incubation of WPE1-NB26-3 cells (stably modified to overexpress the GnRH-R) with SAN1GSC resulted in a robust phosphorylation of ERK1/2 similar to a result observed when the same cells were stimulated by [D-Lys⁶]-GnRH or GSG (lanes 1-3 in Figure 4F). Such an effect was absent when cells were pretreated with a GnRH-R antibody (Figure 4G), suggesting that pERK1/2 activation was a result of direct binding of SAN1GSC to the GnRH-R.

Pharmacokinetic evaluation of SAN1GSC

IP administration of 17 μ mol/Kg of SAN1GSC in mice led to conjugate blood concentrations averaging 20 nM at 0.25 h (Figure 4H). Circulating concentrations of SAN1 formed from the catabolism of SAN1GSC peaked at 0.5 h with a C_{max} of 181 nM at 0.5 h and an AUC_{0-8h} : 0.53 h x μ M. The described experiment indicated that following dosing of SAN1GSC in mice, pharmacologically critical concentrations of SAN1 (exceeding 100 nM) could be achieved in circulation. It should be noted that

the pharmacokinetics of SAN1GSC generating adequate (but low) concentrations of SAN1 sustained over time, was in contrast with the high C_{max} (1100 nM), resulting from the dosing of unconjugated SAN1, a potential risk factor for peripheral toxicity.

In vivo antitumor efficacy of SAN1GSC

Mice bearing established DU145 tumors were dosed with equimolar amounts of SAN1GSC, SAN1, sunitinib and [D-Lys⁶]-GnRH for a period of 20 days. Tumor growth delay was evident in all mice treated with SAN1GSC (Figures 5A and 5B), with an average tumor volume at d20 of $689 \pm 102 \text{ mm}^3$ significantly smaller in comparison to SAN1 ($1010 \pm 114 \text{ mm}^3$, $p < 0.001$) and sunitinib treated mice (1197 ± 248 , $p < 0.001$) or for mice treated with [D-Lys⁶]-GnRH ($1248 \pm 108 \text{ mm}^3$, $p < 0.001$). On d20, the average tumor weight for SAN1GSC treated mice was $0.50 \pm 0.11 \text{ g}$ compared to $0.75 \pm 0.33 \text{ g}$ for SAN1, ($p = 0.038$ vs SAN1GSC), $0.91 \pm 0.27 \text{ g}$ for sunitinib, ($p = 0.003$ vs SAN1GSC) and $0.82 \pm 0.22 \text{ g}$ for [D-Lys⁶]-GnRH treated mice ($p = 0.003$ vs SAN1GSC). All treatments were well tolerated with no noticeable body weight loss or overt toxicity compared to the vehicle group (figure S.I.5). To investigate if SAN1GSC dosing increased the drug payload to the tumor site, concentrations of SAN1, and of SAN1 derived from SAN1GSC administration were determined in blood and tumors in samples obtained 1h post-dose after d20 of treatment (Figure 5C). Measurements of SAN1 at the tumor tissue revealed approximately four times higher SAN1 in SAN1GSC treated mice compared to SAN1 treated mice (113 ± 35 versus $31 \pm 8 \text{ nM}$), with a tumor/blood (t/b) ratio for SAN1 formed from SAN1GSC of 0.55 versus 0.16 for SAN1 treated mice.

In vivo target modulation studies

Histological examination of H&E sections revealed a poorly differentiated high Gleason CaP. IHC analysis in tumor sections using antibodies against Ki-67 and

CD31 showed a marked reduction in cell proliferation and reduced angiogenesis in SAN1GSC treated compared to SAN1, sunitinib or [D-Lys⁶]-GnRH treated mice (Figure 5D). The Ki-67-assessed PI of mice treated with SAN1GSC were $21.5 \pm 2.7\%$, ($P < 0.001$, treated/untreated PI ratio = 0.416), for SAN1 $51.9 \pm 3.7\%$ ($P > 0.01$, treated/untreated PI ratio = 1.005), and for sunitinib $51.5 \pm 3.9\%$ ($P > 0.01$, treated/untreated PI ratio = 0.998) respectively. The average number of CD31+ cells in tumor sections of mice treated with SAN1GSC were 12.7 ± 3.5 , for SAN1 32.14 ± 11 , for sunitinib 30.03 ± 7 and for [D-Lys⁶]-GnRH 28.1 ± 5.4 (Figure 5D). Finally, results from the panel of 39 kinases revealed a marked downregulation of pAKT (Ser473), pERK1/2 and pS6 only in SAN1GSC treated mice compared to all other treatments (Figure 5E). We performed IHC analysis on tissue sections of treated mice against the pS6 protein, in parallel with its activating kinase (RPS6KB1). Reduced levels of phosphorylation were observed for both proteins only in the SAN1GSC treated mice (Figure 5F). Direct inhibition of RPS6KB1 from SAN1GSC was subsequently verified in a cell-free assay, with a calculated IC₅₀ of 337 ± 72 nM (Figure 5G).

Toxicity evaluation of SAN1GSC

The cardiotoxicity of sunitinib (29,30) was assessed and compared to treatment with SAN1GSC, SAN1 by measurements of the cardiac LV function in C57BL/6 mice. Initially we verified that cardiotoxicity related to sunitinib becomes established and reaches a plateau, at one week following treatment. This effect was observed at the efficacious (100 μ mol/Kg) and the non-efficacious dose of sunitinib (9.17 μ mol/Kg) but not in vehicle, as measured by the % FS change from baseline measurements (Figure 6A-B). One week of daily IP equimolar administrations of SAN1GSC and SAN1 demonstrated that SAN1GSC had a minimal, non-significant reduction in % FS

compared to its baseline levels (from 46.79 ± 0.55 to 44.99 ± 0.73) as opposed to a statistically significant % FS reduction following equimolar dosing of SAN1 (from 48.22 ± 0.46 to 46.29 ± 0.60 , $p=0.01$) or equimolar dosing of sunitinib (from 46.35 ± 0.70 to 42.58 ± 0.62 , $p=0.0001$) as shown in Figure 6C.

Hematological analyses of drug treated C57BL/6 mice demonstrated that SAN1GSC did not affect white blood cell (WBC) populations, with only a mild erythrocytosis observed in [D-Lys⁶]-GnRH and SAN1GSC treated mice (figure S.I.6). Thus SAN1GSC was the least toxic of the molecules evaluated under the described conditions.

Discussion

The active targeting of GnRH-R expressing tumors with GnRH based therapeutics is a promising field in the area of personalized treatment. Such a strategy may overcome off-target toxicity in tandem with continuous efficacy due to persistent expression of the GnRH-R on CaP cells, despite prolonged exposure to GnRH agonists (6). A better understanding of CaP microenvironment biology (36) and the central role of angiogenic kinases in tumor growth (37) led us to investigate an alternative strategy by combining sunitinib, a small antiangiogenic molecule with the targeting peptide [D-Lys⁶]-GnRH. Sunitinib has been extensively used in the clinic for the treatment of solid tumors with a known mechanism of action (32) and known off-target cardiotoxicity (38). We hypothesized that conjugation of sunitinib to [D-Lys⁶]-GnRH would deliver the multikinase inhibitor to the site of action, reducing off-target effects and the dose required for efficacy.

Due to the lack of “linkable” free groups of sunitinib, we rationally designed and synthesized five analogs that maintained their efficacy but could also be coupled to

different ligands, expanding their therapeutic potential to other cancer types.

Molecular docking analysis revealed that all SANs assumed a bound conformation similar to sunitinib while remaining efficacious at the low nanomolar scale.

Evaluation of our data combined with facile chemical synthesis singled-out SAN1 as the lead compound for further development using an *in vivo* CRPC xenograft animal model.

SAN1 treatment was well tolerated and proved efficacious in inhibiting tumor growth by reduced CD31 and Ki-67 cells in treated animals, suggesting that inhibition of angiogenesis was at least one mechanism by which SAN1 achieved its efficacy.

Building on the efficacy of SAN1, we investigated whether linking of [D-Lys⁶]-GnRH to SAN1 would lead to an enhanced delivery of the active molecule to the tumor site. SAN1GSC was generated followed by comprehensive *in vitro* and *in silico* evaluation. SAN1GSC maintained its antiangiogenic and cytotoxic properties with IC₅₀ values similar to those of unconjugated SAN1.

Following dosing of SAN1GSC, the detectable levels of free circulating SAN1 in the blood were low, possibly a desirable feature expected to minimize peripheral toxicities. SAN1GSC was well tolerated and proved efficacious in our CRPC xenograft model. Importantly, measurements of SAN1 in tumor sample specimens showed approximately four times higher levels of intracellular SAN1 released from SAN1GSC than levels of SAN1 delivered following SAN1 dosing. A deeper mechanistic insight of the efficacy observed with SAN1GSC was provided by the direct inhibition of the RPS6KB1 enzyme, a molecule linked to CaP aggressiveness and metastasis (39,40). Sunitinib has a reported low nM binding affinity for RPS6KB1 (41) a putative target for the development of new drugs (42). Our finding that *in vivo* inhibition of RPS6KB1 was achieved only in SAN1GSC treated mice was

presumably due to the enhanced targeting of the tumor microenvironment by the conjugate.

SAN1GSC contains the potent [D-Lys⁶]-GnRH agonist peptide, and it is possible that it exerts an additional central effect through the pituitary in the described dosing scheme, leading to the lowering of gonadal hormone levels (31).

Considering that GnRH agonists are typically used for the CRPC treatment in combination with other drugs (*e.g.*, docetaxel, abiraterone), a dual pharmacological approach based on a conjugate monotherapy resulting into intratumoral and circulating testosterone ablation coupled with inhibition of angiogenesis locally, might provide additional benefit in the clinic. Since it is not clear how such an approach would alleviate the problem of resistance to treatment that often develops through mechanisms involving ligand dependent or ligand independent androgen receptor signalling, future studies may be needed to address this hypothesis (40). Our finding that SAN1GSC inhibited RPS6KB1, a molecule with an important role in CRPC and the upregulated PI3K-mTOR-S6 pathway (40), is further encouraging in terms of its clinical potential.

Importantly, SAN1GSC appeared to have a minimal cardiotoxic and hematotoxic effect in treated mice compared to sunitinib and SAN1 in our dosing scheme.

Elevations of blood pressure that might contribute to cardiac dysfunction were not detected following dosing of sunitinib and its analogues, verifying previously published reports (22). However we did observe a reduction in the %FS in mice treated with the various molecules. The reduction of the %FS in SAN1 and sunitinib was not detrimental enough to cause a phenotypic cardiac alteration, but it was statistically significant compared to their corresponding baseline measurements, as opposed to SAN1GSC. Additionally SAN1GSC did not affect WBC populations or

other hematological parameters measured. Mild erythrocytosis was observed in the [D-Lys⁶]-GnRH and SAN1GSC treated mice, possibly linked to the agonist effects of the [D-Lys⁶]-GnRH moiety and temporary increase of testosterone levels (flare effect), an effect that has been reported with GnRH agonists in the clinic (43). One limitation of the current study is the lack of SAN1GSC evaluation in other clinically relevant models, where CaP is either orthotopically generated, or by using patient derived xenografts which reflect the heterogeneity within different cancer histotypes. These studies will assess the efficacy of SAN1GSC in the metastatic setting, where several small molecules often do fail despite initial success in the primary tumor.

In conclusion, we have generated a series of novel linkable antiangiogenic compounds to treat various forms of cancer based on the clinically successful drug sunitinib. We demonstrated for the first time a direct conjugation of a sunitinib analog to a peptide moiety generating a minimally cardiotoxic compound, efficacious at a lower dose than equimolar amounts of sunitinib and able to achieve a four-fold enhanced delivery/benefit to the tumor. The concept is certainly applicable to other solid tumor types expressing the GnRH-R or even to other types of receptors by altering the targeting peptide.

Acknowledgments

We would like to thank Dr Zainol Harun, pathologist of Island Hospital Penang Malaysia, for characterization of the tumors, Ms Anna Agapaki for tissue sectioning and Ms Efi Panagouli for assistance with hematology studies.

References

1. Harmsen S, RJ K. Kinase Inhibitor Conjugates. *Current Pharmaceutical Design* 2012;18(20).
2. Tai W, Shukla RS, Qin B, Li B, K. C. Development of a peptide-drug conjugate for prostate cancer therapy. *Molecular Cancer Therapeutics* 2011;8(3):901-12.
3. Sievers EL, P S. Antibody-Drug Conjugates in Cancer Therapy. *Annual Review of Medicine* 2013;64:15-29.
4. Lewis Phillips GD, Li G, Dugger DL, Crocker LM, Parsons KL, Mai E, et al. Targeting HER2-positive breast cancer with trastuzumab-DM1, an antibody-cytotoxic drug conjugate. *Cancer Res* 2008;68(22):9280-90.
5. Hynes NE, Lane HA. ERBB receptors and cancer: the complexity of targeted inhibitors. *Nat Rev Cancer* 2005;5(5):341-54.
6. Liu SV, Schally AV, Hawes D, Xiong S, Fazli L, Gleave M, et al. Expression of receptors for luteinizing hormone-releasing hormone (LH-RH) in prostate cancers following therapy with LH-RH agonists. *Clin Cancer Res* 2010;16(18):4675-80.
7. Karampelas T, Argyros O, Sayyad N, Spyridaki K, Pappas C, Morgan K, et al. GnRH-Gemcitabine conjugates for the treatment of androgen-independent prostate cancer: pharmacokinetic enhancements combined with targeted drug delivery. *Bioconjugate Chemistry* 2014;25(4):813-23.
8. Emons G, Gorchev G, Harter P, Wimberger P, Stähle A, Hanker L, et al. Efficacy and Safety of AEZS-108 (LHRH Agonist Linked to Doxorubicin) in Women With Advanced or Recurrent Endometrial Cancer Expressing LHRH Receptors: A Multicenter Phase 2 Trial (AGO-GYN5). *International Journal of Gynecological Cancer* 2014;24(2):260-65.
9. Liu SV, Tsao-Wei DD, Xiong S, Groshen S, Dorff TB, Quinn DI, et al. Phase I, Dose-Escalation Study of the Targeted Cytotoxic LHRH Analog AEZS-108 in Patients with Castration- and Taxane-Resistant Prostate Cancer *Clinical Cancer Research* 2014.
10. Limonta P, Marelli MM, Mai S, Motta M, Martini L, RM M. GnRH Receptors in Cancer: From Cell Biology to Novel Targeted Therapeutic Strategies *Endocrine Reviews* 2012;33(5):784-811.

11. Millar R, Newton C. Current and future applications of GnRH, kisspeptin and neurokinin B analogues. *Nature Reviews Endocrinology* 2013;9(8):451-66.
12. Morgan K, Stewart AJ, Miller N, Mullen P, Muir M, Dodds M, et al. Gonadotropin-releasing hormone receptor levels and cell context affect tumor cell responses to agonist in vitro and in vivo. *Cancer Research* 2008;68(15):6331-40.
13. White CD, Stewart AJ, Lu ZL, Millar RP, K. M. Antiproliferative effects of GnRH agonists: prospects and problems for cancer therapy. *Neuroendocrinology* 2008;88(2):67-79.
14. Dondi D, Moretti RM, Montagnani Marelli M, Pratesi G, Polizzi D, Milani M, et al. Growth-inhibitory effects of luteinizing hormone-releasing hormone (LHRH) agonists on xenografts of the DU 145 human androgen-independent prostate cancer cell line in nude mice. *International Journal of Cancer* 1998;76(4):506-11.
15. Al-Husein B, Abdalla M, Trepte M, Deremer DL, PR. S. Antiangiogenic therapy for cancer: an update. *Pharmacotherapy* 2012;32(12):1095-111.
16. Mendel DB, Laird AD, Xin X, Louie SG, Christensen JG, Li G, et al. In vivo antitumor activity of SU11248, a novel tyrosine kinase inhibitor targeting vascular endothelial growth factor and platelet-derived growth factor receptors: determination of a pharmacokinetic/pharmacodynamic relationship. *Clinical Cancer Research* 2003;9(1).
17. Sun L, Liang C, Shirazian S, Zhou Y, Miller T, Cui J, et al. Discovery of 5-[5-fluoro-2-oxo-1,2-dihydroindol-(3Z)-ylidenemethyl]-2,4-dimethyl-1H-pyrrole-3-carboxylic acid (2-diethylaminoethyl)amide, a novel tyrosine kinase inhibitor targeting vascular endothelial and platelet-derived growth factor receptor tyrosine kinase. *Journal of Medicinal Chemistry* 2003;46(7):1116-9.
18. Michaelson MD, Oudard S, Ou YC, Sengeløv L, Saad F, Houede N, et al. Randomized, placebo-controlled, phase III trial of sunitinib plus prednisone versus prednisone alone in progressive, metastatic, castration-resistant prostate cancer. *Journal of Clinical Oncology* 2014;32(2):76-82.
19. Bergh J, Bondarenko IM, Lichinitser MR, Liljegren A, Greil R, Voytko NL, et al. First-line treatment of advanced breast cancer with sunitinib in combination with docetaxel versus docetaxel alone: results of a prospective, randomized phase III study. *Journal of Clinical Oncology* 2012;30(9):921-9.

20. Brooks C, Sheu T, Bridges K, Mason K, Kuban D, Mathew P, et al. Preclinical evaluation of sunitinib, a multi-tyrosine kinase inhibitor, as a radiosensitizer for human prostate cancer. *Radiation Oncology* 2012;7(154):1-9.
21. Force T, Kolaja KL. Cardiotoxicity of kinase inhibitors: the prediction and translation of preclinical models to clinical outcomes. *Nat Rev Drug Discov* 2011;10(2):111-26.
22. Chintalgattu V, Rees ML, Culver JC, Goel A, Jiffar T, Zhang J, et al. Coronary microvascular pericytes are the cellular target of sunitinib malate-induced cardiotoxicity. *Sci Transl Med* 2013;5(187):187ra69.
23. Caballero J, Muñoz C, Alzate-Morales JH, Cunha S, Gano L, Bergmann R, et al. Synthesis, in silico, in vitro, and in vivo investigation of 5-^[11C]methoxy-substituted sunitinib, a tyrosine kinase inhibitor of VEGFR-2. *European Journal of Medicinal Chemistry* 2012;58:272-80.
24. Chen KT, Fang z, yANG z, K G. Design, Synthesis and Biological Evaluation of Sunitinib Analogues to Improve Aqueous Solubility. *Advanced Material Research* 2014;749:350-53.
25. Dolman MEM, Harmsen S, Pieters EHE, Sparidans RW, Lacombe M, Szokol B, et al. Targeting of a platinum-bound sunitinib analog to renal proximal tubular cells. *International Journal of Nanomedicine* 2012;7: 417—33
26. London CA, Malpas PB, Wood-Follis SL, Boucher JF, Rusk AW, Rosenberg MP, et al. Multi-center, placebo-controlled, double-blind, randomized study of oral toceranib phosphate (SU11654), a receptor tyrosine kinase inhibitor, for the treatment of dogs with recurrent (either local or distant) mast cell tumor following surgical excision. *Clinical Cancer Research* 2009;15(11):3856-65.
27. Noh GT, Kim MH, Suh JY, Song Y, Lee CK, Baek JH, et al. Sunitinib--CLIO conjugate: a VEGFR/PDGFR-targeting active MR probe. *Molecular Imaging and Biology* 2014;16(3).
28. Patyna S, Laird AD, Mendel DB, O'farrell AM, Liang C, Guan H, et al. SU14813: a novel multiple receptor tyrosine kinase inhibitor with potent antiangiogenic and antitumor activity. *Molecular Cancer Therapeutics* 2006;7:1774-82.
29. Prakash CR, Theivendren P, S R. Indolin-2-Ones in Clinical Trials as Potential Kinase Inhibitors: A Review. *Pharmacology & Pharmacy*, 2012;3(1):62-71.

30. Laird AD, Vajkoczy P, Shawver LK, Thurnher A, Liang C, Mohammadi M, et al. SU6668 Is a Potent Antiangiogenic and Antitumor Agent That Induces Regression of Established Tumors. *Cancer Research* 2000;60(15):4152-60.
31. Katsila T, Balafas E, Liapakis G, Limonta P, Montagnani Marelli M, Gkoutelias K, et al. Evaluation of a Stable Gonadotropin-Releasing Hormone Analog in Mice for the Treatment of Endocrine Disorders and Prostate Cancer *The Journal of Pharmacology and Experimental Therapeutics* 2011;336(3):613-23.
32. Kumar R, Crouthamel MC, Rominger DH, Gontarek RR, Tummino PJ, Levin RA, et al. Myelosuppression and kinase selectivity of multikinase angiogenesis inhibitors. *British Journal of Cancer* 2009;101(10):1717-23.
33. Breitkopf SB, Yuan M, Pihan GA, Asara JM. Detection of a rare BCR-ABL tyrosine kinase fusion protein in H929 multiple myeloma cells using immunoprecipitation (IP)-tandem mass spectrometry (MS/MS). *Proc Natl Acad Sci U S A* 2012;109(40):16190-5.
34. Psarras S, Mavroidis M, Sanoudou D, Davos CH, Xanthou G, Varela AE, et al. Regulation of adverse remodelling by osteopontin in a genetic heart failure model. *Eur Heart J* 2012;33(15):1954-63.
35. Remko M, Bohaç A, Kovacikova L. Molecular structure, pKa, lipophilicity, solubility, absorption, polar surface area, and blood brain barrier penetration of some antiangiogenic agents. *Struct Chem* 2011;22(3):635-48.
36. Karlou M, Tzelepi V, E. E. Therapeutic targeting of the prostate cancer microenvironment. *Nature Reviews Urology* 2010;7(9):494-509.
37. Niu G., X. C. Vascular Endothelial Growth Factor as an Anti-angiogenic Target for Cancer Therapy. *Current Drug Targets* 2010;11(8):1000-17.
38. Aparicio-Gallego G, Blanco M, Figueroa A, García-Campelo R, Valladares-Ayerbes M, Grande-Pulido E, et al. New insights into molecular mechanisms of sunitinib-associated side effects. *Molecular Cancer Therapeutics* 2012;10(11):2215-23.
39. Cai C, Chen QB, Han ZD, Zhang YQ, He HC, Chen JH, et al. miR-195 Inhibits Tumor Progression by Targeting RPS6KB1 in Human Prostate Cancer. *Clin Cancer Res* 2015.

40. Karantanos T, Corn PG, Thompson TC. Prostate cancer progression after androgen deprivation therapy: mechanisms of castrate resistance and novel therapeutic approaches. *Oncogene* 2013;32(49):5501-11.
41. Karaman MW, Herrgard S, Treiber DK, Gallant P, Atteridge CE, Campbell BT, et al. A quantitative analysis of kinase inhibitor selectivity. *Nat Biotechnol* 2008;26(1):127-32.
42. Pearce LR, Alton GR, Richter DT, Kath JC, Lingardo L, Chapman J, et al. Characterization of PF-4708671, a novel and highly specific inhibitor of p70 ribosomal S6 kinase (S6K1). *Biochem J* 2010;431(2):245-55.
43. Bachman E, Feng R, Travison T, Li M, Olbina G, Ostland V, et al. Testosterone suppresses hepcidin in men: a potential mechanism for testosterone-induced erythrocytosis. *J Clin Endocrinol Metab* 2010;95(10):4743-7.

Figure Legends

Figure 1

Synthetic route of sunitinib analogues and physicochemical properties. **(A)** Synthesis of sunitinib analogs 1-5 from the available acid intermediate 1. Reagents and conditions: (a) DMF, EDCI, HOBt, NEt₃, rt; (b) CH₂Cl₂, TFA, rt. **(B)** Key properties and MS conditions for the sunitinib analogues.

Figure 2

In silico, *in vitro* and pharmacokinetic evaluation of the synthesized SANs. **(A)** Docking for sunitinib and SAN1-SAN5 with estimated inhibition constants (K_i in nM). Molecular model of the VEGFR-2 complex with SAN1 **(B)** Summary of *in vitro*

kinase activity in multiple RTKs in the presence of sunitinib or SANs 1-5, (\pm SD). **(C)** Cell based autophosphorylation assay for PDGFR- β and VEGFR-2 for sunitinib or SANs 1-5, (\pm SD). **(D)** MTT cytotoxicity assay in a panel of cell lines, (\pm SD). **(E)** Pharmacokinetic evaluation of the most potent SANs versus sunitinib in mice. N.D: Not Determined, N.A: Not Active

Figure 3

Efficacy of SAN1 and sunitinib in NOD/SCID mice xenografted with the CRPC DU145 cell line. **(A)** Tumor growth inhibition. Mice were dosed (IP) daily with SAN1 (100 μ mol/Kg), sunitinib (50 and 100 μ mol/Kg), or vehicle. **(B)** Average tumor weight at day of sacrifice (d19) between treatment groups. **(C)** Average intratumoral drug concentrations were measured by LC-MS/MS at 2h post a final dose on d19, \pm SD. **(D)** Histological sections of xenograft tissue harvested on the day of sacrifice (d19). Brown indicates DAB reaction product. Representative x40 fields are shown. Scale bar: 50 μ m. **(E)** Heat map analysis showing the *In vivo* phosphorylation status of 39 kinases on drug versus vehicle treated mice.

Figure 4

Generation and evaluation of the conjugate SAN1GSC. **(A)** Synthesis of SAN1GSC from SAN1 and [D-Lys⁶]-GnRH. **Reagents and conditions:** (a) DMF, DMAP, NEt₃, rt; (b) [D-Lys⁶]-GnRH, DMF, HATU, NiPr₂Et. **(B)** Molecular representation of the energy minimized model of VEGFR-2 catalytic domain (blue surface) in complex with the SAN1GSC conjugate (sticks) that is color-coded with cyan carbons for the sunitinib analog SAN1 and orange for the [D-Lys⁶]-GnRH peptide. The inset illustrates a closeup view of the ATP-binding site with the SAN1 moiety of the conjugate (cyan) and the key interacting residues (orange). Intermolecular hydrogen bonds are shown with dotted lines and the other atom colors are blue for N, red for O,

yellow for S and pink for F. The predicted inhibition constants K_i for three kinase receptors are given in nM. **(C)** Summary of *in vitro* kinase activity ($IC_{50} \pm SD$) in various RTKs in the presence of SAN1GSC and [D-Lys⁶]-GnRH. **(D)** Cell based autophosphorylation assay for PDGFR- β and VEGFR-2 in the presence of SAN1GSC and [D-Lys⁶]-GnRH. **(E)** MTT cytotoxicity assay in a panel of cell lines. **(F)** SAN1GSC activates the ERK1/2 pathway through binding to the GnRH-R. **(G)** Phosphorylation of ERK1/2 following treatment with SAN1GSC, [D-Lys⁶]-GnRH or GSG is absent when cells are pretreated for 30 min with an antibody against the human GnRH-R. **(H)** Pharmacokinetic evaluation of SAN1GSC. Drug Levels of SAN1GSC and SAN1 formed from its breakdown were monitored by LC-MS/MS. The area under the curve (AUC) for each treatment was calculated as a measure of drug exposure over time. N.A: Not active

Figure 5

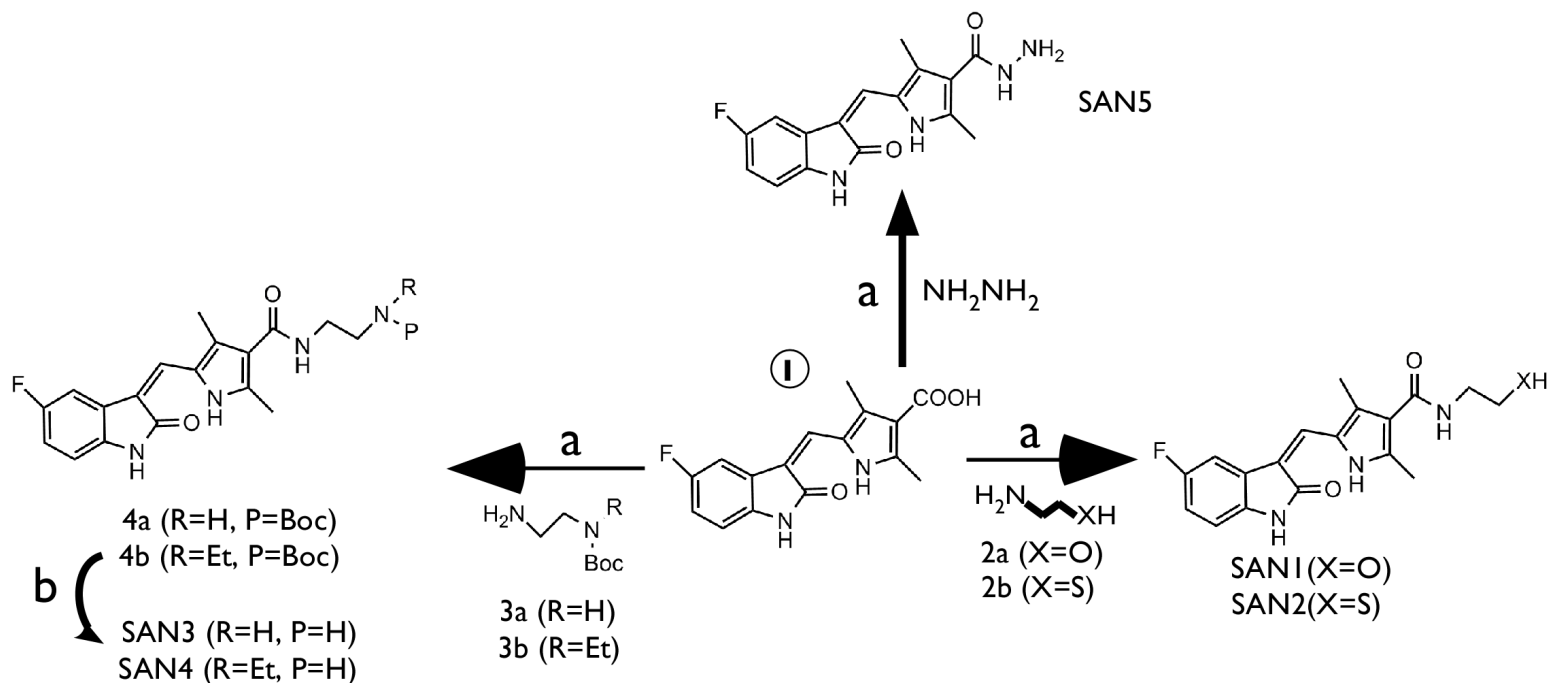
Efficacy of SAN1GSC in NOD/SCID mice xenografted with the CRPC DU145 cell line. **(A)** Efficacy of SAN1GSC (9.17 $\mu\text{mol/Kg}$), versus equimolar amounts of SAN1, sunitinib and [D-Lys⁶]-GnRH in NOD/SCID mice xenografted with DU145 cells. **(B)** Average tumor weight at day of sacrifice (d20) between treatment groups. **(C)** Average intratumoral drug levels were measured by LC-MS/MS at one hour post a final dose on d20, $\pm SD$. SAN1 formed from the SAN1GSC is four times higher than SAN1 treated mice, despite the fact that blood levels are similar, resulting in a higher blood/tumor ratio on SAN1GSC treated mice. **(D)** Histological sections of xenograft tissue harvested on day of sacrifice (d20). **(E)** Heat map analysis showing the *in vivo* phosphorylation status of 39 kinases on drug versus vehicle treated mice at one hour post a final dose on d20. **(F)** Immunohistochemical analysis on sections of xenograft tissue harvested on day of sacrifice (d20) against pS6 and pRPS6KB1. A marked

reduction of phosphorylation for both proteins is seen only in SAN1GSC treated mice. For each IHC photo brown indicates DAB reaction product, with representative x40 fields shown. Scale bar: 50 μm (G) Summary of the *in vitro* kinase activity in RPS6KB1 in the presence of various molecules ($\text{IC}_{50} \pm \text{SD}$).

Figure 6

Cardiac LV function echocardiography measurements in C57BL/6 mice treated daily with IP doses of the various compounds. (A) Representative M-mode echocardiograms at one week following treatment. (B) Percentage FS reduction compared to baseline, for sunitinib treated mice at 9.17 and 100 $\mu\text{mol/Kg}$ for a total period of four weeks. (C) Percentage FS reduction compared to baseline levels, at one week of treatment with equimolar doses of SAN1 and SAN1GSC, as well as 100 $\mu\text{mol/Kg}$ of SAN1. Data are expressed as mean \pm SE and a $p < 0.05$ value was considered statistically significant.

A



B

R	Compound	MW	cLogP	Total Polar Surface Area (Å ²)	Precursor Ion (m/z, amu)	MS/MS (m/z, amu)
	<i>Sunitinib</i>	398.4	2.99	73.47	399.4	283, 326
	<i>SAN1</i>	343.4	0.96	90.46	344.4	283
	<i>SAN2</i>	359.4	2.01	70.23	360.3	283
	<i>SAN3</i>	342.4	1.04	96.25	343.5	283, 326
	<i>SAN4</i>	370.2	1.87	82.26	371.5	283, 326
	<i>SAN5</i>	314.1	0.93	96.25	315.4	257, 270

Figure 1

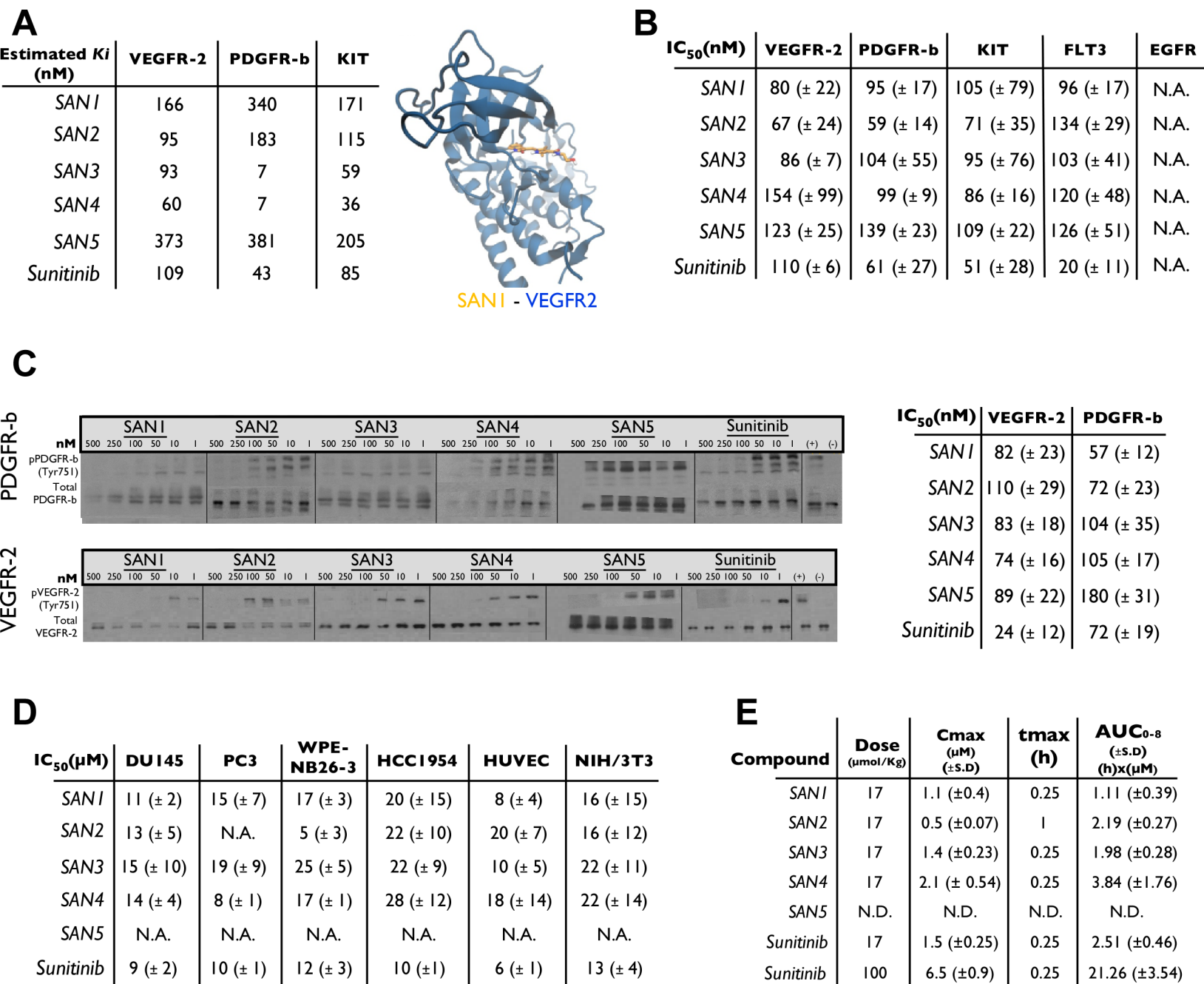
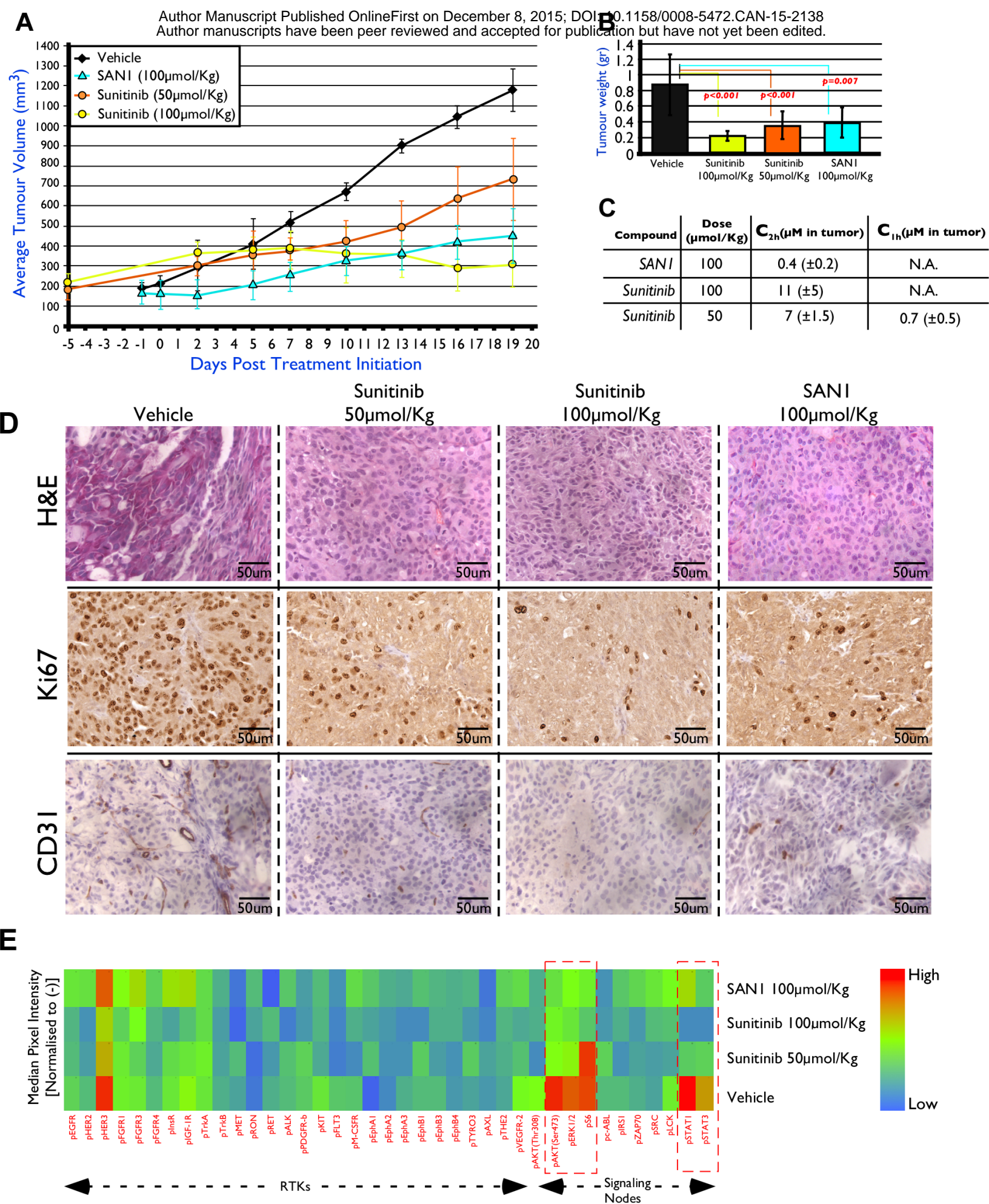
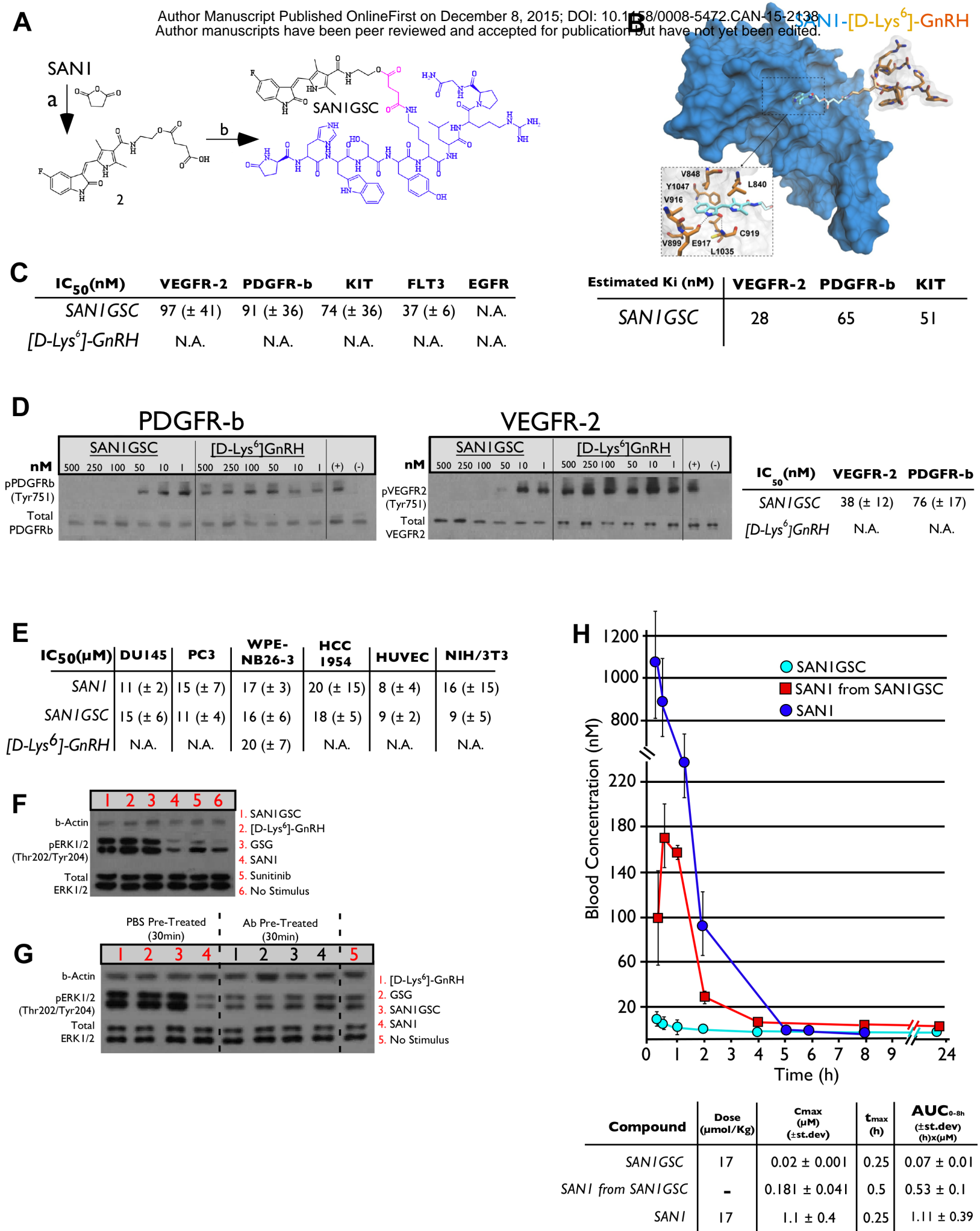
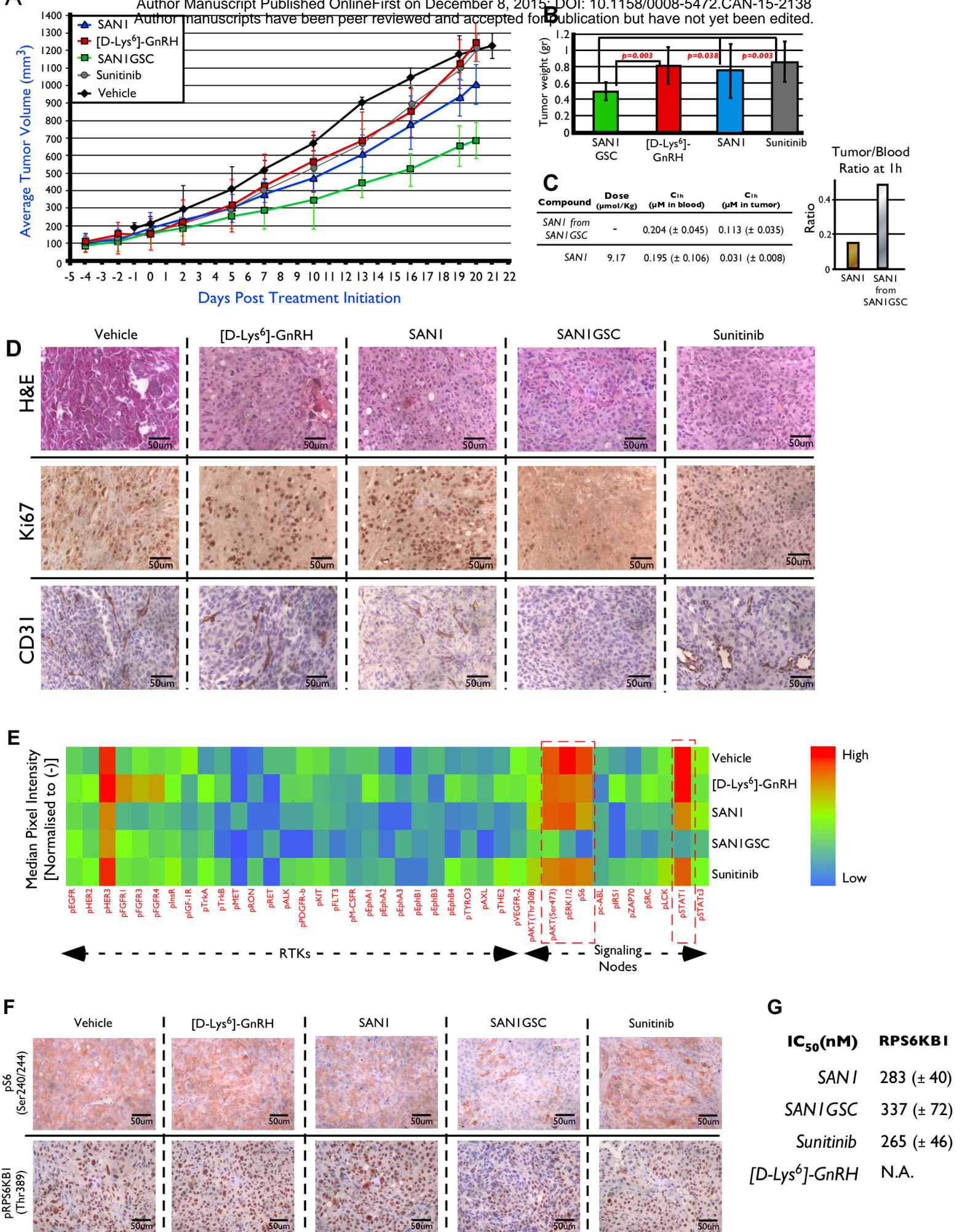


Figure 2







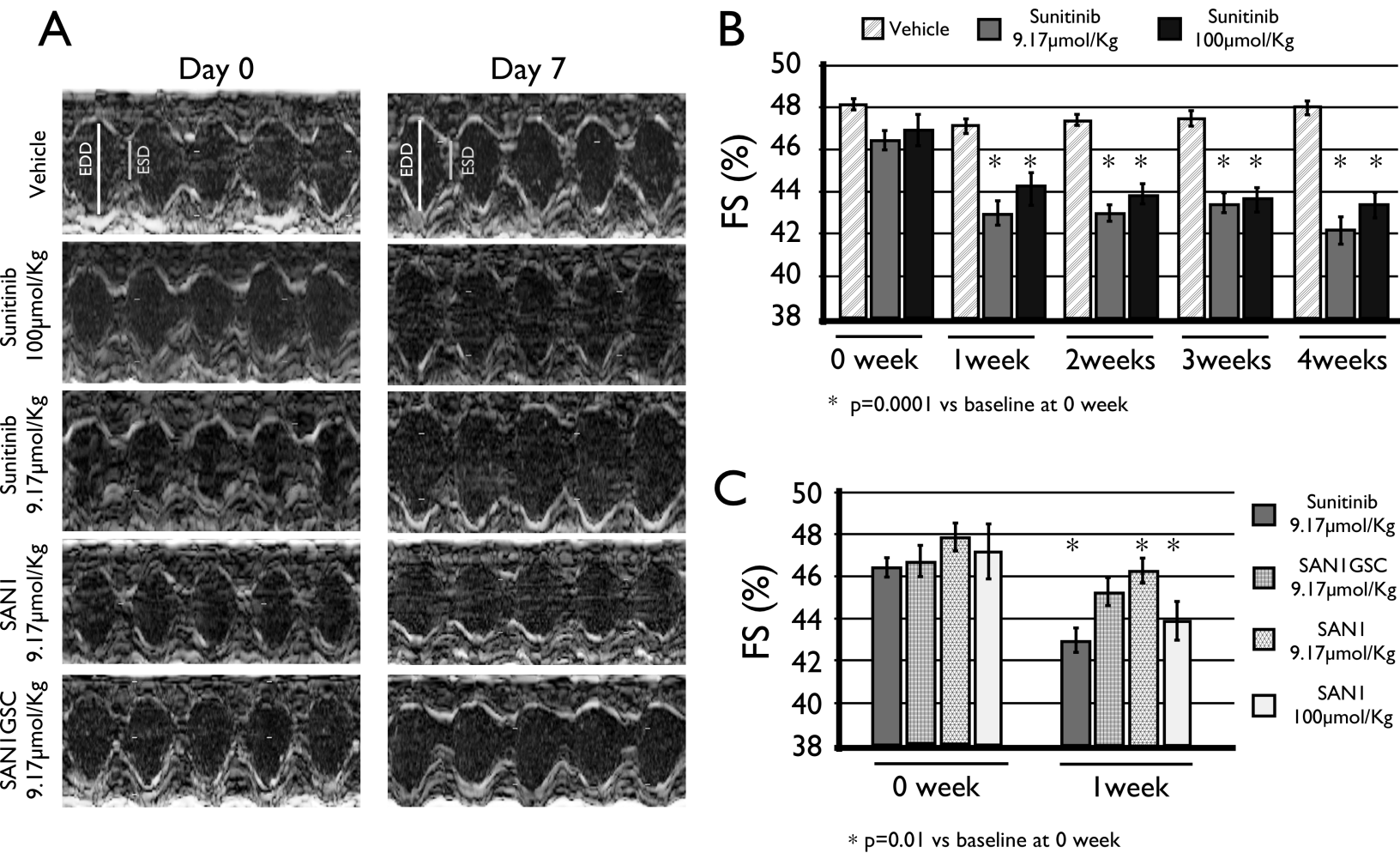


Figure 6

Cancer Research

The Journal of Cancer Research (1916–1930) | The American Journal of Cancer (1931–1940)

Peptide-drug conjugate GnRH-sunitinib targets angiogenesis selectively at the site of action to inhibit tumor growth

Orestis Argyros, Theodoros Karampelas, Xenophon Asvos, et al.

Cancer Res Published OnlineFirst December 8, 2015.

Updated version	Access the most recent version of this article at: doi: 10.1158/0008-5472.CAN-15-2138
Supplementary Material	Access the most recent supplemental material at: http://cancerres.aacrjournals.org/content/suppl/2015/12/08/0008-5472.CAN-15-2138.DC1.html
Author Manuscript	Author manuscripts have been peer reviewed and accepted for publication but have not yet been edited.

E-mail alerts [Sign up to receive free email-alerts](#) related to this article or journal.

Reprints and Subscriptions To order reprints of this article or to subscribe to the journal, contact the AACR Publications Department at pubs@aacr.org.

Permissions To request permission to re-use all or part of this article, contact the AACR Publications Department at permissions@aacr.org.